Kinetic Reaction Rates for Consumption of Pyrolytic Graphite by Combustion Gases

J. W. Schaefer,* H. Tong,† and R.J. Bedard‡
Acurex Corporation, Mountain View, Calif.

An experimental program using an arc plasma generator was conducted to determine the kinetic mass consumption rate of pyrolytic graphite in simulated propellant atmospheres. These results, which include a wide range of gas species partial pressures and ablation rates, were successfully correlated using an equation with a functional form determined from phenomenological considerations. These correlations were in turn incorporated as an integral part of a prediction procedure which includes the simultaneous consideration of boundary-layer diffusion, equilibrium gas-phase chemistry, kinetically controlled surface chemistry, sublimation, indepth heat conduction and, surface mass transfer. The end product of this program was a procedure for predicting pyrolytic graphite ablation rates in rocket motor nozzles under conditions where surface kinetic effects are important.

Introduction

THE thermal protection of a solid rocket motor nozzle requires the use of high-performance materials such as graphites and refractories. For high-performance motors it is essential that a smooth nozzle contour be maintained throughout the firing time. In addition, the effective throat diameter should ideally be invariant. Pyrolytic graphite in both *a-b* and *c* plane orientations has demonstrated low recession rates and has been identified as an attractive throat insert material. The erosion rates, especially in the *a-b* plane orientation, have been observed to be much less than that predicted by equilibrium surface thermochemistry. The clear implication is that the erosion rate is reaction rate limited. To design a rocket nozzle, the designer must be able to accurately predict the erosion rate of the nozzle materials so that a realistic balance can be achieved between weight, performance, and cost. This capability for pyrolytic graphite has not been available. This paper therefore addresses the problem of thermochemical erosion of pyrolytic graphites and the development of procedures for the analytic prediction of their erosion rates in any propellant environment.

Reaction Characteristics

For solid propellants of current interest, combustion temperatures (T_o) range from 3000°R to 8000°R. At these conditions, the constituent ingredients of typical solid propellants combust to form varying amounts of gaseous H_2O, CO_2, H_2, CO, N_2, and HCl plus condensed metal oxides such as Al_2O_3. As an example, the elemental and molecular compositions for APG 112D propellant are given in Tables 1 and 2. Note that the large amount of hydrogen in the propellant precludes the formation of significant amounts of either molecular or elemental oxygen.

From chemical equilibrium considerations, the determination of those species which may actively contribute to graphite ablation in the solid rocket nozzle can be made. Of the possible overall reactions, only the following have sufficiently large equilibrium constants in the temperature range of interest to warrant investigation:

$$C^* + H_2O \rightarrow CO + H_2 \qquad (1)$$

Table 1 Elemental composition of APG 112D propellant

Element	Atomic weight	Relative composition (gram-atoms/gram of propellant)
Hydrogen	1.008	0.032219
Carbon	12.011	0.005649
Nitrogen	14.008	0.005366
Oxygen	16.000	0.022486
Sodium	22.991	Trace
Aluminum[a]	26.980	0.010130
Sulphur	32.066	Trace
Chlorine	35.457	0.005396

[a] 27.3% aluminum mass fraction.

Table 2 Molecular composition of APG 112D at anticipated chamber conditions[a]

Chemical Species	Mole fraction[b]
Primary species	
H_2	0.3285
CO	0.1820
$Al_2O_3^{*c}$	0.1393
H_2O	0.1076
HCl	0.0933
H	0.0924
N_2	0.0890
Other species	
AlCl	0.0291
$AlCl_2$	0.0201
HO	0.0179
Cl	0.0174
CO_2	0.0071
Al	0.0038
$AlHO_2$	0.0029
O	0.0028
NO	0.0016
AlO	0.0015
Al_2O	0.0013
others	0.0030

[a] $T_o = 7020°R$, $P_o = 1000$ psia.
[b] Mole fraction defined as: moles of species per gas phase mole.
[c] Condensed phase (liquid): mass concensed/mass gas = 0.735; also system molecular weight = 33.5 grams/gas-phase mole.

Presented as Paper 74-1056 at the AIAA/SAE 10th Propulsion Conference, San Diego, California, October 21-23, 1974; submitted December 2, 1974; revision received March 28, 1975. This work was supported by the Air Force Rocket Propulsion Laboratory under Contract FO4611-69-C-0081. The authors wish to acknowledge the valuable contributions of M.R. Wool, A.J. Murphy, K.J. Clark, and J.J. Reese Jr.

Index categories: Material Ablation; Thermochemistry and Chemical Kinetics; Solid and Hybrid Rocket Engines.

*Assistant General Manager, Aerotherm Division.
†Senior Staff Engineer, Aerotherm Division.
‡Manager, Propulsion Systems, Aerotherm Division.

$$C^* + CO_2 \rightarrow 2CO \quad (2)$$

$$2C^* + H_2 \rightarrow C_2H_2 \quad (3)$$

The reaction of surface carbon with other reactants such as oxygen would also be included in the above list if the reactants were present in significant quantity and had a reaction rate such that the carbon consumption rate was non-negligible. Some degree of caution is necessary in the selection of the reaction equations since reactants which are important at low temperatures need not also be important at high temperatures. In addition, reactions which are important for one class of graphites need not also be important for the other classes of graphites.

The erosion of carbon by H_2O, CO_2, and H_2 has been the subject of a number of experimental investigations such as those of Refs. 1-10. In addition, carbon erosion by oxygen has been the subject of Refs. 11-19. This data has not been widely applied to rocket motor design because the data was not correlated into a useful form, or the data did not provide sufficient information about the complex interactions of reactants and inhibitors such as HCl or CO.

The phenomena associated with rate-controlled reactions between a propellant combustion product stream and a pyrolytic graphite nozzle surface are shown shematically in Fig. 1. Characterization of these complicated events by such a simplistic diagram serves to illustrate the various aspects of the surface response which must be considered in the definition of suitable ablation rate prediction procedures. Any of these five steps in the ablation process could control the rate of surface removal.

When the surface removal rate is controlled by the diffusion of the reactive or product species, the surface reaction rates must be proceeding fast enough to offer negligible resistance to the formation of ablation products. For the important surface reactions, no specific rate expressions are required since product concentrations are determined only from chemical equilibrium and mass transfer considerations. Reactions rates are, of course, finite but the rates of diffisuion are sufficiently slow that equilibrium (i.e., infinite rates) can be used with no compromise in prediction accuracy. In addition, the prediction of ablation is computationally more simple in this situation. For the case where the diffusional rates exceed reaction rates, the equilibrium assumption becomes inaccurate and rate relations must be developed for the controlling step (or steps) in the surface reaction process.

Rate Expressions

The characteristics of the various reactions between propellant combustion products and graphitic materials and the effects of other species in the combustion products on the reactions is very complex. The type of analytical expression needed to predict the various response trends is certainly not clear from the diverse presentations available in the literature. The characterization of Fig. 1 indicates that a formulation which accounts for an active site limit on the ablation rate is very reasonable. A Langmuir-type expression[20] which contains a summation of reactive species partial pressures in the numerator and one plus the summation of inhibiting or competing species in the denominator seems to be consistent with the various observed data trends and response model requirements. Additionally, a relation is necessary which characterizes the energy level of the reactive species, as a function of termperature, required to make the reaction as characterized in Fig. 1 proceed to completion. Kinetic theory suggests a probability function which may be expressed in the form of an Arrhenius type function.[20] In general terms, the reaction rate expression may be written as follows:

$$r = \sum_i \left[B_i e^{-E_{ai}/RT_w} \left[p_i / \prod_j (1 + \sum_j k_j p_j) \right] \right] \quad (4)$$

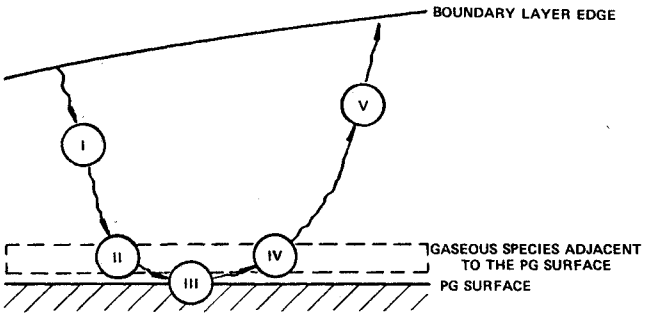

Fig. 1 Reaction rate controlled ablation characterization. I. Diffusion of the reactive species from the boundary-layer edge to the region of the PG surface. II. Adsorption of the reactive species to an active site on the PG surface. III. Formation of reaction products at the PG surface. IV. Desorption of reaction products from the PG surface. V. Diffusion of reaction products into the boundary layer.

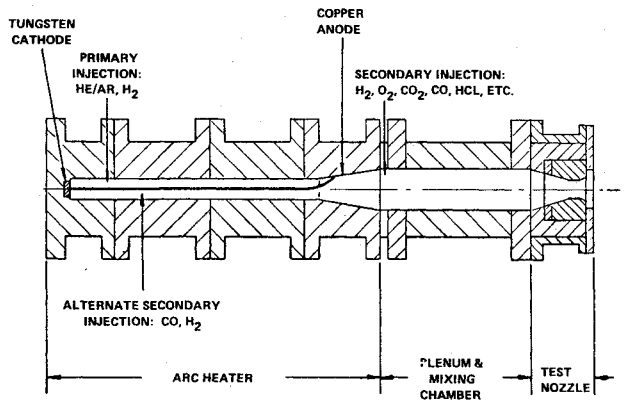

Fig. 2 Overall test configuration.

where i = reactive species, j = inhibiting (or competing) species, B = pre-exponential (steric factor), E_a = activation energy, R = universal gas constant, T_w = surface temperature, p = partial pressure, k = weight factor which may or may not be a function of temperature, and r = overall surface reaction rate.

Experimental Procedure

The Aerotherm 1-Mw constricted arc plasma generator (APG), Fig. 2, was used to perform the tests. The unit consists of tungsten cathode, insulated constrictor segments, copper anode, plenum and mixing chamber, and axisymmetric nozzle test section. In the APG, energy is added to the primary test gas via a steady electric arc discharge, the arc being struck from a tungsten cathode to the downstream diverging anode. The primary gas is introduced tangentially through an insulator separating the cathode well from the first insulated constrictor segment and/or along the constrictor column to provide stable, high-voltage operation. The secondary gas is introduced in the upstream end of the plenum-mixing chamber downstream of the arc to yield the desired final gas composition and to insure equilibrium of the primary and secondary gases before they exhaust through the axisymmetric test section.

To satisfy the test program requirements, a large number of test gas compositions and test conditions were employed in the test program. The test gases which were arc heated in the APG, individually or in combination, were argon-helium mixture, hydrogen, carbon monoxide, oxygen, and nitrogen. The test gases which were introduced into the plenum chamber just downstream of the arc, individually or in combination, were hydrogen, carbon monoxide, oxygen, and hydrogen chloride. The actual mix of these gases in terms of type and introduction location was determined by the desired test conditions.

The argon-helium mixture was 50-50 by mole and served as the inert carrier gas in those tests for which an inert carrier gas was employed. This gas, which closely duplicates the molecular weight and specific heat of typical combustion products, is an attractive gas for APG performance, and provides reasonable reactant mole fractions and therefore partial pressures. In all gas systems which included H_2O, this gas was generated by combustion in the plenum chamber via the reaction $H_2 + \frac{1}{2}O_2 \rightarrow H_2O$. In all gas systems which included CO_2, this gas was also generated by combustion via this reaction $CO + \frac{1}{2}O_2 \rightarrow CO_2$. This approach provided a higher temperature capability and in the case of H_2O eliminated the problems of introducing steam into the APG.

Test conditions were varied by varying test gas compositions and for a given composition by varying the electical power input. Two different test sample throat diameters were also used to provide test condition variations through a factor of about two changes in pressure.

Test Nozzle Configurations

The test configuration was an axisymmetric nozzle as shown in Fig. 3. The pyrolytic graphite insert test sections formed the throat region of the nozzle. The pyrolytic graphite washer immediately upstream of the test section insert insured a smooth transition into the insert and held the boundary-layer trip. This trip was employed to insure turbulent flow, and therefore high-transfer coefficients, in the throat. The test section insert was retained by a crushable high-temperature insulator. The test section could therefore expand as required while retention was still maintained. The PG coated inserts were designed with 0.005-in. clearance between the o.d. and the nozzle housing i.d. The insert was wrapped with magic mending tape to fill this gap. In this manner, the insert o.d. was properly restrained but this restraint caused no unusually high stresses during the test; as the insert got hot and expanded radially, the tape decomposed to accomodate this expansion.

The test sections were miniature axisymmetric nozzles with throat diameters of either 0.35 or 0.45 in. All coated inserts were supplied by the Atlantic Research Corporation. The nominal coating thickness for both large and small diameter inserts were as follows: entrance—0.026 in; throat—0.030 in; and exit—0.013 in. The substrate was AGSR graphite in all cases. All coated nozzle inserts were tested as-deposited except two; these two were also annealed. The PG washer nozzles were fabriacted from material supplied by Super-Temp Company except for one; which was material from Pyrogenics, Inc. The basic design employed thin washers in the throat region backed up by low conductivity graphite foam. This minimized the conduction loss from the surface and therefore maximized the surface temperature.

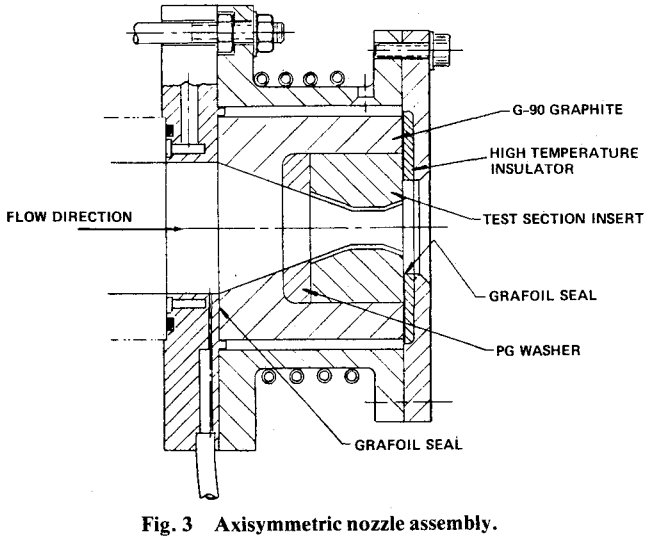

Fig. 3 Axisymmetric nozzle assembly.

The measurements made to characterize the test conditions and material response were: test conditions—gas total enthalpy, chamber pressure, and cold wall heat flux; material response—surface temperature history, surface recession, and qualititative surface condition.

Data Analysis Procedure

Since surface kinetic rates are determined by the local partial pressures of chemical species, a necessary part of the data analysis procedure is to determine these partial pressures. In particular, the region of interest is the throat region of the sample nozzle since the characteristics of this region can be the most easily defined. A fundamental assumption of the data analysis procedure is that gas-phase thermochemical equilibrium is always achieved even though the gases are not in equilibrium with the surface. This assumption is valid because the high gas temperatures and high pressures lead to very rapid gas-phase reaction rates. The surface species partial pressures are then determined by the following steps: 1) The state of the gases at the edge of the boundary layer is determined by an isentropic expansion from the plenum state to the choked Mach = 1 condition. 2) The mass-transfer coefficient of the boundary layer at the throat is determined from the experimentally measured heat-transfer coefficient via an analogy between the heat- and mass-transfer coefficients. 3) The surface temperature is obtained directly from the experimental data and the surface ablation rate $\dot{m}_C$ is obtained from the measured surface recession rate and the known pyrolytic graphite density. 4) Steps 2 and 3 provide sufficient information for an open system chemical equilibrium solution to determine the species partial pressures adjacent to the surface. Note that kinetic rates are implicit in Step 3 by the specification of the ablation rate. All thermochemical calculations are performed with the Aerotherm Chemical Equilibrium (ACE) code, which is described in Ref. 21.

Test conditions were calibrated with a steady-state water-cooled calorimeter nozzle of identical configuration to the test nozzle. The heat flux at the throat, as determined by the temperature rise of the water passing through the calorimeter section, is related to the heat-transfer coefficient by the equation

$$(\rho_e u_e C_H)_{cw} = q_{cw}/(H_r - H_w) \tag{5}$$

where $\rho_e u_e C_H$ is the heat-transfer coefficient and *cw* indicates cold-wall conditions. H_w, the enthalpy of the gas adjacent to the wall, is determined from an ACE calculation and H_r the recovery enthalpy is determined from the relationship

$$H_r = H_o - 0.112\,(H_o - H_.) \tag{6}$$

where H_o is the stagnation enthalpy and $H_.$ is the enthalpy at the edge of the boundary layer. Since the heat-transfer coefficient is a function of temperature as well as of small variations in arc operating conditions, the heat-transfer coefficient in Eq. (5) must be corrected to obtain the correct value for the actual ablation conditions. This correction is accomplished by scaling with the ratio of the transfer coefficients, as predicted by the Bartz equation[22] for the ablation and calorimeter tests. The mass-transfer coefficient is determined from the Spalding relationship

$$\rho_e u_e C_M / \rho_e u_e C_H = Le^{2/3} \tag{7}$$

where Le is the Lewis number. This mass-transfer coefficient and the experimental surface ablation rate and surface temperature are then used in an open system ACE calculation to determine the species partial pressures at the ablating surface.

Given the surface partial pressures, the remaining part of the data analysis is to correlate the data in a useful formulation. Based on the functional form given in Eq. (4), some knowledge of past data, and some intuition, the following kinetic carbon consumption model was selected.

$$\dot{m}_C = \sum_i \left[B_i e^{-E_{ai}/RT_w} \Big/ \prod_n \left[1 + \sum_j A_{j,n} p_j \right] \times \left(p_i - \Pi p_{\text{prods},i}/K_{pi} \right) \right] \tag{8}$$

where the last term in parens accounts for the reverse reaction related to the ith reactant, K_p being the equilibrium constant for that reaction. The $\prod_n$ terms correspond to inhibitors which can be any species including the reactants themselves. The possibility of different constants (including zero) for different temperature regimes was also allowed. The model has the Arrhenius form for the temperature dependence of the consumption rate, and the Langmuir form for the inhibition effect. Additional complications to the model could have been added to make it more general but were not considered warranted by the quantity and accuracy of the test results and the already significant generality of the model. Note also that in order to reduce the number of empirical constants to be determined, the k_j's, which would normally be of the Arrhenius form, are replaced by constants $A_{j,n}$. The data analysis now reduces to the nontrivial task of determining an appropriate set of $A_{j,n}$, B_i, and E_{ai} so as to obtain a suitable correlation of the data.

Analysis of Experimental Data

Experimental data was obtained for pyrolytic graphite in both the *a-b* and *c* plane orientations, however, most of the data was obtained for the *a-b* orientation since it was known to have a low ablation rate.§ The procedure was therefore to first analyze the *a-b* plane data to determine the constants $A_{j,n}$ and assume that they were independent of the pyrolytic graphite orientation. The constants B_i and E_{ai} were, however, allowed to be different.

a-b Plane Pyrolytic Graphite

The complete set of data for *a-b* plane pyrolytic graphite is shown in Fig. 4 in terms of the log of the carbon consumption rate vs $1/T_w$. Note that in this form the data has little significance since species partial pressures were widely variant. The figure is shown only to indicate the quantity and temperature range of the data. For the record, the range of partial pressures for species of interests are shown in Table 3.

In the analysis of the data the H_2O and CO_2 reactions were considered first. This initial activity demonstrated that the H_2O and CO_2 reactions interacted rather immediately such that they could both be effectively correlated by the same kinetic model. For H_2O and CO_2, Eq. (8) therefore reduced to the form

$$\dot{m}_c = Be^{-E_a/RT_w} \Big/ \prod_n (1 + \sum_j A_{j,n} p_j)_n \times \sum_i \left(p_i - \Pi p_{\text{prods},i}/K_{pi} \right) \quad i = H_2O, CO_2 \tag{9}$$

This correlation also had the virtue that it applied over the entire temperature range. Note that the correlation could be reasonably well developed in the absence of consideration of the H_2 reaction since a significant number of test points were available for which the H_2 effect was small, either because of low or moderature temperature when the H_2 reaction rate is negligible or because the quantity of H_2 was small. The inhibitors in Eq. (9) (subscript j) were found to be HCl, H_2O, CO_2, CO, and H_2. Note that the reactants themselves are included in this list.

This correlation of the data does not exhibit a rate maximum nor multiple temperature regimes for CO_2 as indicated by the other investigations. From this point, all results including those for which the H_2 reaction was significant were analyzed to finalize the H_2O/CO_2 correlation and to develop the H_2 correlation. The H_2 contribution to the consumption rate was of course also constrained to the form of Eq. (8) but not unexpectedly was found to have a different activation energy and pre-exponential factor than the H_2O/CO_2 correlation. The inhibiting species for the H_2 reaction were also found to be different; they are H_2O, CO_2, and CO. Note that the reactant itself and HCl are not inhibitors of the H_2 reaction. Note also that neither of the three reactions are affected by N_2; it behaves as an inert gas.

The final kinetic model defined by a correlation of all test results and constrained by the form of Eq. (8) is

$$\dot{m}_C = \left[\frac{MCL \times k_{H_2}}{1 + p_{H_2O} + p_{CO_2} + p_{CO}} \right] \left[p_{H_2} - \frac{p_{C_2H_2}}{K_{pH_2}} \right] + \left[\frac{MCL}{1 + p_{H_2O} + p_{CO_2} + p_{CO} + p_{H_2}} \right] \left[\frac{1}{1 + 3p_{HCl}} \right] \times \left[\left[p_{H_2} - \frac{p_{CO} p_{H_2}}{K_{pH_2O}} \right] + \left[p_{CO_2} - \frac{p_{CO}^2}{K_{pCO_2}} \right] \right] \tag{10}$$

where $MCL = 151 \exp(-46{,}000/RT_w)$ lbm-atm/ft^2 sec, and $MCL \times k_{H_2} = 18.4 \exp(-55{,}500/RT_w)$ lbm-atm/ ft^2 sec. Note that all the $A_{j,n}$ were set at 1.0 (atm^{-1}) except for the HCl term which was set at 3.0 (atm^{-1}). The quality of the correlation in terms of MCL versus $1/T_w$ is shown in Fig. 5.

C-Plane Pyrolytic Graphite

The data for *c*-plane oriented pyrolytic graphite is shown in Fig. 6 and the ranges of surface pressures and mass con-

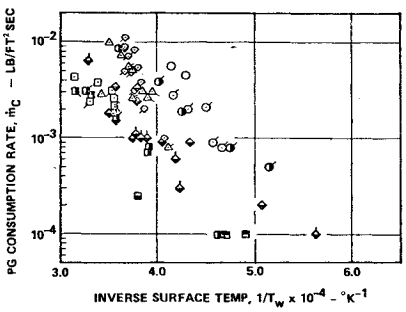

Fig. 4 Summary of all *a-b* plane results.

Table 3 Surface species partial pressure and mass consumption rate range for pyrolytic graphite data

a-b plane
$0 \le p_{H_2O} \le 2.30$ atm
$0 \le p_{H_2} \le 4.68$ atm
$0 \le p_{HCl} \le 1.02$ atm
$0 \le p_{CO_2} \le 0.50$ atm
$0 \le p_{CO} \le 2.13$ atm
$0.0001 \le \dot{m}_C \le 0.0110$ lbm/ft^{2}sec
c plane
$0 \le p_{H_2O} \le 1.33$ atm
$0.62 \le p_{H_2} \le 2.26$ atm
$0 \le p_{HCl} \le 0.34$ atm
$0 \le p_{CO_2} \le 0.22$ atm
$0 \le p_{CO} \le 1.73$ atm
$0.0003 \le \dot{m}_C \le 0.024$ lbm/ft^{2}sec

§In practice, however, *a-b* plane pyrolytic graphite is deposited on a graphite substrate and differential thermal expansion may lead to the establishment of destructive thermal stresses.

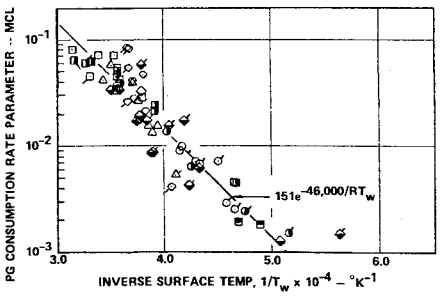

Fig. 5 Arrhenius/ Langmuir-type correlation for all *a-b* plane results.

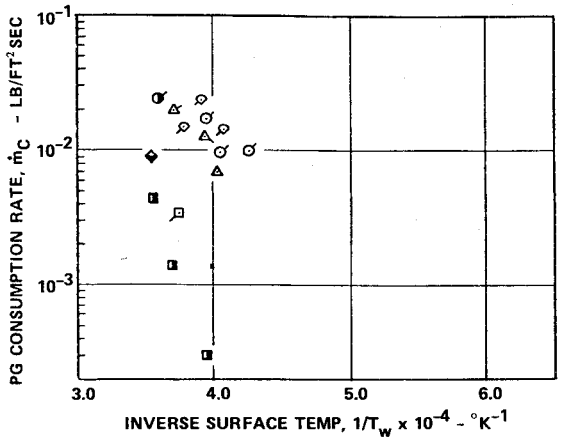

Fig. 6 Summary of all *c* plane results.

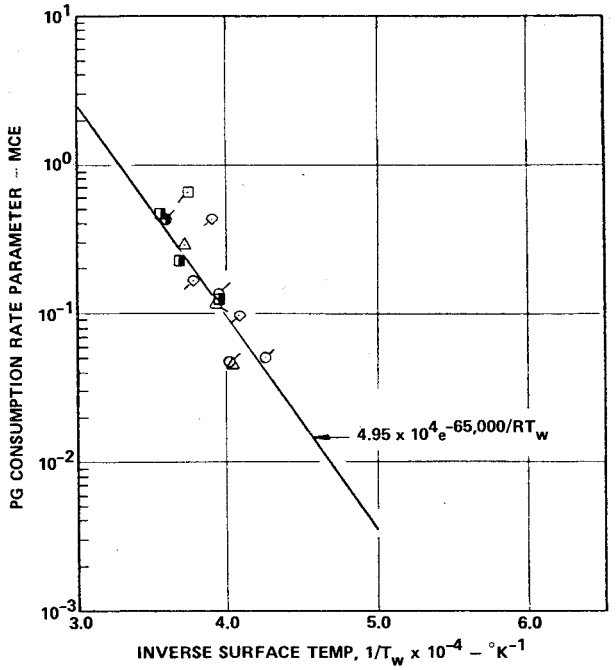

Fig. 7 Arrhenius/Langmuir type correlation for all *c* plane results.

sumption rates for this data are shown in Table 3. Because substantially less data was obtained for this orientation it was not practical to perform a full data correlation as was done for *a-b* plane pyrolytic graphite. Instead, it was assumed that the $A_{j,n}$ were invariant between the two pyrolytic graphite orientations so that only the Arrhenius functions were to be determined. In this way, the best correlation based on Eqs. (10) yielded $MCE = 4.95 \times 10^4 \exp(-65{,}000/RT_w)$ lbm-atm/ft^{2}sec, $MCE \times k_{H_2} = 2.5 \times 10^7 \exp(129{,}500/RT_w)$ lbm-atm/ft^2 where *MCL* is replaced by *MCE*. The quality of the correlation is shown in Fig. 7. Clearly, because of the small amount of data and the smaller temperature range of the data (compared to *a-b* plane pyrolytic graphite) the confidence level in the accuracy of the correlation of the *c*-plane orientation is somewhat lower than that for the *a-b* plane orientation.

Application of Correlations to Graphite Ablation Performance Predictions

Since the correlations are based on local partial pressures, rather than freestream values, and they include the effects of active site occupation by nonreacting species, they can become an integral part of a prediction procedure for the performance of pyrolytic graphite in solid rocket motor propellant environments. In addition, since the functional form of the correlations are based on analytic and phenomenological considerations, the correlations should be applicable even at conditions which are beyond the range of the experimental data. This is particularly true for the *a-b* plane correlations; however, because of the small amount of *c*-plane data, there should be some reservations about extrapolating outside of the experimental data range. In fact, it is currently established that the *a-b* plane correlation leads to very accurate predictions of ablation performance, whereas predictions with the *c*-plane correlation has met with mixed results.

For full gas phase and surface thermochemical equilibrium (not reaction rate controlled), a well established analytic procedure has been validated for ablation performance predictions. This procedure treats the coupled effects of boundary-layer flow, chemistry, mass consumption and in-depth heat conduction in a parametric manner based on transfer coefficients. In general, the following steps are required: 1) definition of the freestream flow; 2) definition of the boundary-layer flow conditions; 3) determination of the thermochemical state in the region immediately adjacent to and including the surface; and 4) determination of the in-depth transient thermal response of the ablator. For virtually all situations of interest, the freestream state, at any given instant of time, is unaffected by boundary-layer events so that these conditions can be determined a priori from expected propellant operating conditions. Boundary-layer events, however, are intimately coupled to the ablation rate which, in turn, is coupled to the transient in-depth material response. The treatment of this coupled boundary-layer-surface-in-depth response by a single computer code is possible but not practical. An accepted practical procedure developed at Aerotherm has been to treat the coupling parametrically via boundary-layer transfer coefficients for heat and mass. In this treatment, the nonablating transfer coefficients are determined for the boundary-layer flow (Step 2) and a set of equilibrium thermochemical tables (Step 3) are generated with the ACE code to obtain relationships between surface temperature, normalized mass ablation rate ($B' = \dot{m}/\rho_e u_e C_M$), and chemical energy dissipation. These tables then contain, in a parametric form, all of the boundary-layer and surface-thermochemistry information which then serve as constraints for the in-depth calculations (Step 4). Note that changes in the mass-transfer coefficient due to surface blowing are also included in the analysis procedure.

For nonequilibrium surface chemistry (reaction rate controlled), Step 3 is replaced by a set of thermochemistry tables which include the effects of surface kinetics. These tables are easily generated by a code (GASKET)[23] which is a sister code to ACE. GASKET contains the above surface kinetics correlations as built-in functions. However, in general, any set of Arrhenius-like functions can be specified as input data. In addition, the effects of surface sublimation reactions are also included. Over the past few years, GASKET has received wide acceptance in the solid rocket motor industry as a general code to treat surface graphite kinetics, however, it has become clear that more data is required for *c* plane pyrolytic graphite and other graphitic materials such as silicon carbide, codeposited pyrolytic graphite, carbon-carbon composites and metal-modified graphites. Many of these materials will be examined in a current AFRPL-sponsored program.

Conclusion

Pyrolytic graphite ablation rates are strongly dependent on the type and quantity of chemical species in the propellant combustion products, the surface temperature achieved, and the pyrolytic graphite type (i.e., *a-b* or *c* plane). The experimental test results obtained to quantify this dependence were correlated using an equation with a functional form determined from phenomenological considerations—an Arrhenius/Langmuir-type equation. The application of these results to general propellant systems requires a computer code which incorporates the correlation model and constants, and which includes treatment of boundary-layer diffusion, kinetically controlled surface chemistry, sublimation, and surface mass transfer. The GASKET computer code developed for this purpose has been validated through comparisons to rocket firings, and represents a major improvement in rocket nozzle design capability.

References

[1] Kebler, R.W. and Walsh, P.N., "Principles Governing the Behavior of Solid Materials on Severe High Temperature Environments," Final Rept. UCRI-388, May 1966, Union Carbide Research Institute, Tarrytown, N.Y.

[2] Lewis, J.C., Floyd, I.J., and Cowlard, F.C., "A Laboratory Investigation of Carbon-Gas Reactions of Relevance to Rocket Nozzle Erosion," presented at the 34th meeting (8th colloquium) of the AGARD Propulsion and Energetics Panel, Oct. 1969.

[3] Shevtsov, V.P., Shafer, G.S., Klirikov, G.W., and Al'Tshuler, V.S., "On the Joint Reaction of Carbon Dioxide and Water Vapor with Carbon at Normal and Elevated Pressures," *Trudy Institute Goriuchirh Iskopsemykh,* Vol. 16, 1961, pp. 164-170.

[4] Clarke, J.T. and Fox, B.R., "Reaction of Graphite Filaments with Hydrogen Above 2000°K," *Journal of Chemical Physics,* Vol. 46, Feb. 1967, pp. 827-836.

[5] Lewis, J.C., Floyd, I.J., and Cowlard, F.C., "A Comparative Study of the Gaseous Oxidation of Vitreous Carbon and Various Graphite at 1500-3000°K," Allen Clark Research Center and Beckwith Carbon Report.

[6] Austin, L.G. and Walker, P.L., Jr., "Effect of Carbon Monoxide in Causing Nonuniform Gasification of Graphite by Carbon Dioxide," *AIChE Journal,* Vol. 9, May 1963, pp. 303-306.

[7] King, M.K., "Kinetics of High-Temperature Reactions of Graphite with Carbon Dioxide and Water," *Journal of Spacecraft & Rockets,* Vol. 8, May 1971, pp. 470-474.

[8] Walls, J. and Strickland-Constable, R., "The Reaction Between CO_2 and Graphite at Temperatures Between 1500 and 2100°C, *Carbon,* Vol. 3, Dec. 1965, p. 350.

[9] Clark, J., "Reaction of Graphite and Hydrogen Above 2000°K," *The Application of Plasmas to Chemical Processing,* edited by Baddora and Timmins, MIT Press, Cambridge, Mass., 1967, pp. 132-156.

[10] Schaefer, J.W., Reese, J.J., Jr., and Anderson, L.W., "Determination of Kinetic Rate Constants for the Reaction of Solid Propellant Combustion Products with Pyrolytic Graphite," Rept. 68-31, May 1968, Aerotherm, Mountain View, Calif.

[11] Walls, J.R. and Strickland-Constable, R.F., "Oxidation of Carbon Between 1000-2400°C," *Carbon,* Vol. 1, April 1964, pp. 333-338.

[12] Scala, S.M. and Gilbert, L.M., "Sublimation of Graphite at Hypersonic Speeds," *AIAA Journal,* Vol. 3, Sept. 1965, pp. 1625-1644.

[13] Scala, S.M., "The Ablation of Graphite in Dissociated Air, Part I: Theory," R62SD72, Sept. 1962, Missile and Space Division, General Electric Company, Philadelphia, Pa.

[14] Ong, J.N., Jr., "On the Kinetics of Oxidation of Graphite," *Carbon,* Vol. 2, Dec. 1964, pp. 281-297.

[15] Rosner, D.E. and Allendorf, H.D., "Comparative Studies of the Attack of Pyrolytic Graphite and Isotropic Graphite by Atomic and Molecular Oxygen at High Temperature," May 1967, Paper TP-156, Aerochem Research Labs., Inc., Princeton, N.J.

[16] Horton, W.S., "Oxidation Kinetics of Pyrolytic Graphite," *Proceedings of the Fifth Conference on Carbon,* Vol. 2, Macmillan, New York, 1963, pp. 233-241.

[17] Maahs, H.G., "Kinetic Limitations on the Diffusional Control Theory of the Ablation Rate of Carbon," *Journal of Spacecraft & Rockets,* Vol. 8, Dec. 1971, pp. 1226-1228.

[18] Nagle, J. and Strickland-Constable, R.F., "Oxidation of Carbon Between 1000-2000°C," Proceedings of the Fifth Conference on Carbon, pp. 154-164.

[19] Blyholder, G., Binford, J.S., Jr., and Eyring, H., "A Kinetic Theory for the Oxidation of Carbonized Filaments," *Journal of Physical Chemistry,* Vol. 62, March 1958, pp. 263-267.

[20] Glasstone, S., *The Elements of Physical Chemistry,* Van Nostrand, New York, 1949.

[21] Kendall, R.M., "An Analysis of the Coupled Chemically Reacting Boundary Layer and Charring Ablator, Part V: A General Approach to the Thermochemical Solution of Mixed Equilibrium—Nonequilibrium, Homogeneous or Heterogenerous Systems," CR-1064, June 1968, NSAS (also published as Aerotherm Rept. 66-7, Pt. V).

[22] Bartz, D.R., "A Simple Equation for Rapid Estimation of Rocket-Nozzle Convective Heat-Transfer Coefficients," *Jet Propulsion,* Jan. 1957, p. 49.

[23] User's Manual, "Aerotherm Graphite Surface Kinetics Computer Program," Vols. I-II, Jan. 1972, AFRPL-72-23, Air Force Rocket Propulsion Lab., Wright-Patterson Air Force Base, Ohio.